AFRL-RV-PS-
TP-2015-0011

IMPROVED MULTIPLE-EVENT LOCATION METHODS FOR GROUND-TRUTH COLLECTION
Annual Report

William L. Rodi and Delaine T. Reiter

Department of Earth, Atmospheric, and Planetary Sciences
Massachusetts Institute of Technology, Room 54-219
Cambridge, MA 02139

13 March 2015

Technical Report

AIR FORCE RESEARCH LABORATORY
Space Vehicles Directorate
3550 Aberdeen Ave SE
AIR FORCE MATERIEL COMMAND
KIRTLAND AIR FORCE BASE, NM 87117-5776

DTIC COPY

NOTICE AND SIGNATURE PAGE

AFRL-RV-PS-TP-2015-0011 HAS BEEN REVIEWED AND IS APPROVED FOR PUBLICATION IN ACCORDANCE WITH ASSIGNED DISTRIBUTION STATEMENT.

//SIGNED//	//SIGNED//
Capt. Ashley Green	Dr. Thomas R. Caudill, Acting Chief
Deputy Program Manager, AFRL/RVBYE	AFRL Battlespace Environment Division

REPORT DOCUMENTATION PAGE

Form Approved
OMB No. 0704-0188

1. REPORT DATE *(DD-MM-YYYY)*	**2. REPORT TYPE**	**3. DATES COVERED** *(From - To)*
13-03-2015	Technical Report	04 Sep 2013 – 04 Sep 2014

4. TITLE AND SUBTITLE
IMPROVED MULTIPLE-EVENT LOCATION METHODS FOR GROUND-TRUTH COLLECTION
Annual Report

5a. CONTRACT NUMBER
FA9453-13-C-0279

5b. GRANT NUMBER

5c. PROGRAM ELEMENT NUMBER
62601F

6. AUTHOR(S)
William L. Rodi and [1]Delaine T. Reiter

5d. PROJECT NUMBER
1010

5e. TASK NUMBER
PPM00018801

5f. WORK UNIT NUMBER
EF122779

7. PERFORMING ORGANIZATION NAME(S) AND ADDRESS(ES)
Department of Earth, Atmospheric, and Planetary Sciences
Massachusetts Institute of Technology, Room 54-219
Cambridge, MA 02139

[1]Weston Geophysical Corp
181 Bedford Street, Suite 1
Lexington, MA 02420

8. PERFORMING ORGANIZATION REPORT NUMBER

9. SPONSORING / MONITORING AGENCY NAME(S) AND ADDRESS(ES)
Air Force Research Laboratory
Space Vehicles Directorate
3550 Aberdeen Avenue SE
Kirtland AFB, NM 87117-5776

10. SPONSOR/MONITOR'S ACRONYM(S)
AFRL/RVBYE

11. SPONSOR/MONITOR'S REPORT NUMBER(S)
AFRL-RV-PS-TP-2015-0011

12. DISTRIBUTION / AVAILABILITY STATEMENT
Approved for Public Release; distribution is unlimited. (OPS-15-7410 dtd 11 May 2015)

13. SUPPLEMENTARY NOTES

14. ABSTRACT
The goal of this project is to develop a new methodology for seismic multiple-event locations which can improve the quality of ground-truth event databases. The improvements sought include more complete and rigorous quantification of location uncertainty, better quality control on secondary phase picks associated with ground-truth events, and a greater quantity of events that meet specified ground-truth criteria. To achieve these improvements we are pursuing several enhancements to multiple-event location methodology applicable to earthquake clusters, such as the combined use of local, regional and teleseismic arrival-time data in a unified analysis, and application of a rigorous framework for uncertainty analysis that incorporates more realistic, and generally less restrictive, assumptions about travel-time model errors attributable to unknown velocity variations in the Earth. This report describes the mathematical framework and numerical algorithms we developed in the first year of the project and shows results of preliminary tests we performed with data from Nevada Test Site explosions.

15. SUBJECT TERMS
Seismic Location, Multiple-Event Location, Earthquake Clusters, Ground Truth Seismic Locations, Hypocentroidal Decomposition, Reciprocal Cluster Analysis

16. SECURITY CLASSIFICATION OF:			**17. LIMITATION OF ABSTRACT**	**18. NUMBER OF PAGES**	**19a. NAME OF RESPONSIBLE PERSON**
a. REPORT	**b. ABSTRACT**	**c. THIS PAGE**			Capt. Ashley E. Green
Unclassified	Unclassified	Unclassified	Unlimited	36	**19b. TELEPHONE NUMBER** *(include area code)*

Standard Form 298 (Rev. 8-98)
Prescribed by ANSI Std. 239.18

This page is intentionally left blank.

Table of Contents

List of Figures

List of Tables

This page is intentionally left blank.

1 SUMMARY

The goal of this project is to develop a new methodology for seismic multiple-event location which can improve the quality of ground-truth event databases. The improvements sought include more complete and rigorous quantification of location uncertainty, better quality control on phase picks associated with ground-truth events, and a greater quantity of events that meet specified ground-truth criteria. To achieve these improvements we are pursuing several enhancements to multiple-event location methodology applicable to earthquake clusters, such as the combined use of lo-cal, regional and teleseismic arrival-time data in a unified analysis, and application of a rigorous framework for uncertainty analysis that incorporates more realistic, and generally less restrictive, assumptions about unknown travel-time corrections (model errors) attributable to unknown velocity variations in the Earth.

In the first year of the project we developed the mathematical framework and numerical algorithm for much of our more general approach to multiple-event location. We applied the resulting multiple-event location algorithm to two event clusters: the Rogun earthquake cluster in Tajikistan, one of the clusters in the IASPEI ground-truth database processed with the HDC-RCA method, and 57 explosions in the Pahute Mesa testing area of Nevada Test Site for which ground-truth (GT0) location information is available. Our application to the Rogun cluster demonstrated that our multiple-event location approach emulates the HDC-RCA as a special case of its more general methodology. The application to Pahute Mesa explosions showed that our method can achieve epicentral locations with a median mislocation of 1 km and maximum of 3 km, when outlier suppression techniques we implemented are applied. However, our preliminary tests of a more general stochastic model of travel-time corrections, which uses a full variance-covariance matrix on the corrections as prior information, did not reduce location errors, indicating the need for further work on this element of our approach.

2 INTRODUCTION

Ground-truth seismic events play a crucial role in the development of improved event location methods for nuclear monitoring, both as a source of data for travel-time calibration via velocity tomography or empirical methods, and in the validation of location and calibration procedures. While several non-seismic means for deriving accurate event locations exist (e.g. explosion catalogs, mine blast records, satellite imagery, InSAR signals), the most abundant source of ground-truth information is seismic arrival-time data. Although event-location accuracy achievable from arrival-time data is limited by our knowledge of the Earth's velocity structure, the location accuracy needed for nuclear monitoring applications ($\leq$5 km, or GT5) can be sometimes achieved by applying multiple-event location methods to regional and teleseismic data from a small event cluster, to constrain the relative locations between the events, and using data from a well-distributed network of local stations to constrain the absolute locations of one or more of the events. In particular, the hypocentroidal decomposition (HDC) method (Jordan and Sverdrup, 1981; Engdahl and Bergman, 2001), has been used extensively to develop a large GT5 data base for use by the nuclear monitoring community (Bonda´r *et al.*, 2004; Bonda´r and McLaughlin, 2009).

However, good local seismic networks are not available in all areas of monitoring interest, which motivated Bonda´r *et al.* (2008) to extend the HDC method with reciprocal cluster analysis (RCA) in order to relax the requirements for local data. The resulting HDC-RCA method is a two-step procedure. First, HDC is applied to regional and teleseismic arrivals to determine the relative locations of the events in a cluster (known an cluster vectors). Second, RCA is applied to determine the absolute location of the cluster (cluster hypocentroid) from arrival times observed at one or more local stations. Exploiting travel-time reciprocity, RCA treats the event cluster as a local seismic network which is used to relocate the local stations; the cluster hypocentroid is then derived from the resulting station mislocations. RCA does not require that the local stations be able to determine accurate locations of individual events and thus extends the applicability of the HDC method.

This project is attempting to extend multiple-event location methodology even further with the goal of improving the quality of ground-truth event databases. The improvements sought include more complete and rigorous quantification of location uncertainty, especially for event focal depths and origin times; better quality control on phase picks associated with ground-truth events; and a greater quantity of events that meet specified ground-truth criteria, particularly in areas poorly represented in current databases. To achieve these improvements we are pursuing several en-hancements to multiple-event location methodology applicable to earthquake clusters. A primary enhancement is the combined use of local, regional and teleseismic arrival-time data in a unified analysis in order to extract all information on both absolute and relative event locations that is available in the data. Further, we are applying a rigorous framework for uncertainty analysis to characterize the errors in ground-truth location parameters more completely and assign appropriate ground-truth levels. ur uncertainty approach will incorporate more realistic, and generally less restrictive, assumptions about unknown travel-time corrections attributable to unknown velocity variations in the Earth. The improved treatment of these corrections will potentially reduce location uncertainty and allow the application of multiple-event location analysis to earth uake clusters excluded by current methods, resulting in more ground-truth events.

3 TECHNICAL APPROACH

3.1 Problem Formulation

We are addressing the problem of inferring the location parameters of a set of J seismic events from arrival-time data observed at a network of seismic stations. We let $\mathbf{h}_j$ denote the 4-component vector of hypocentral parameters (including origin time) of the jth event, and let $\mathbf{t}_j$ denote the vector of arrival times observed from that event, noting that the station/phase-type combinations for which times are observed can differ among events. The multiple-event location problem is to solve for the $\mathbf{h}_j$ from

$$\mathbf{t}_j = F_j(\mathbf{h}_j; \mathbf{m}) + \mathbf{e}_j, \quad j = 1, \ldots, J \tag{1}$$

where F_j is a forward modeling function which adds the origin time of the jth event to travel times predicted from its hypocenter, and where $\mathbf{e}_j$ is a vector of measurement errors in the arrival-time picks. The travel times predicted by F_j are assumed to be the theoretical times through the Earth's seismic velocity structure, as described by a model parameter vector $\mathbf{m}$.

In practice, the Earth's velocity is not known and travel-time calculation is done with a refer-ence model $\mathbf{m}^{\text{ref}}$. We thus replace eq. (1) with

$$\mathbf{t}_j = F_j(\mathbf{h}_j; \mathbf{m}^{\text{ref}}) + \mathbf{c}_j + \mathbf{e}_j, \quad j = 1, \ldots, J \tag{2}$$

where each vector $\mathbf{c}_j$ contains travel-time corrections, given by (3)

$$\mathbf{c}_j = F_j(\mathbf{h}_j; \mathbf{m}) - F_j(\mathbf{h}_j; \mathbf{m}^{\text{ref}}).$$

The correction vectors clearly depend on the models $\mathbf{m}$ and $\mathbf{m}^{\text{ref}}$ as well as their respective event hypocenters, although our notation does not show these dependences. It is important to note that, if the $\mathbf{c}_j$ are assumed to be zero, effectively ignoring the inadequacy of the reference velocity model, the multiple-event location problem decouples across events and can be solved by locating each event separately from its own data, i.e. performing single-event location on each event.

The original multiple-event location methods (e.g. Jordan and Sverdrup, 1981; Pavlis and Booker, 1983) assumed that the travel-time corrections do not depend on event location, which effectively assumes that the events are in a tight cluster with location differences between events being much less than event-station distances. This assumption can be stated as

$$\mathbf{c}_j = \mathbf{S}_j \boldsymbol{\gamma} \tag{4}$$

where the vector $\boldsymbol{\gamma}$ contains a set of "master" corrections (one for each station/phase-type combination observed for at least one event) and the matrix $\mathbf{S}_j$, containing ones and zeros as its elements,

selects the appropriate subset of master corrections for the jth event. Substituting (4) into (2) yields

$$\mathbf{t}_j = F_j(\mathbf{h}_j; \mathbf{m}^{\text{ref}}) + \mathbf{S}_j\boldsymbol{\gamma} + \mathbf{e}_j, \quad j = 1, \ldots, J. \tag{5}$$

Further, the original multiple-event location methods effectively treated the master corrections as deterministic unknowns, unconstrained by prior information. Different methods solved eqs. (5) with different numerical techniques, some solving explicitly for $\boldsymbol{\gamma}$ (in conjunction with the $\mathbf{h}_j$) and others eliminating $\boldsymbol{\gamma}$ as a "nuisance" parameter and solving explicitly only for the $\mathbf{h}_j$.

3.1.1 The HDC-RCA Method

The baseline for this project is the hypocentroidal decomposition (HDC) method as implemented by Engdahl and Bergman (2001) and extended with reciprocal cluster analysis (RCA) by Bondár *et al.* (2008). The HDC method decomposes the event hypocenter vectors into a *hypocentroid* $\bar{\mathbf{h}}$ and cluster vectors $\Delta\mathbf{h}_j$, defined by

$$\bar{\mathbf{h}} = \frac{1}{J}\sum_{j=1}^{J} \mathbf{h}_j \tag{6}$$

$$\Delta\mathbf{h}_j = \mathbf{h}_j - \bar{\mathbf{h}}. \tag{7}$$

The cluster vectors determine the pattern of event locations within the event cluster while the hypocentroid determines the absolute location of the cluster.

Jordan and Sverdrup (1981) showed that, in allowing unconstrained travel-time corrections, some information about the event locations is lost, primarily information about the hypocentroid. This can be understood by linearizing the forward functions F_j about $\bar{\mathbf{h}}$ and approximating eq. (5) as

$$\mathbf{t}_j \approx F_j(\bar{\mathbf{h}}; \mathbf{m}^{\text{ref}}) + \mathbf{B}_j\,\Delta\mathbf{h}_j + \mathbf{S}_j\boldsymbol{\gamma} + \mathbf{e}_j, \quad j = 1, \ldots, J \tag{8}$$

where $\mathbf{B}_j$ is the Jacobian (partial derivative matrix) of $F_j(\mathbf{h}, \mathbf{m})$ with respect to $\mathbf{h}$, evaluated at $\mathbf{h} = \bar{\mathbf{h}}$ (and $\mathbf{m} = \mathbf{m}^{\text{ref}}$). Now let us define a master forward function $\mathcal{F}$ which, for any given hypocenter, predicts arrival times for the distinct station/phase combinations existing in the multi-event data set. Given the selection matrices $\mathbf{S}_j$, we can write

$$F_j(\bar{\mathbf{h}}; \mathbf{m}^{\text{ref}}) = \mathbf{S}_j\mathcal{F}(\bar{\mathbf{h}}; \mathbf{m}^{\text{ref}}) \tag{9}$$

and thus, letting $\mathbf{B}$ be the Jacobian of $\mathcal{F}$ with respect to its hypocenter argument,

$$\mathbf{B}_j = \mathbf{S}_j\mathbf{B}. \tag{10}$$

We can now write eq. (8) as

$$\mathbf{t}_j \approx \mathbf{S}_j\Big[\mathcal{F}(\bar{\mathbf{h}}; \mathbf{m}^{\text{ref}}) + \mathbf{B}\,\Delta\mathbf{h}_j + \boldsymbol{\gamma}\Big] + \mathbf{e}_j, \quad j = 1, \ldots, J. \tag{11}$$

When the cluster vectors $\Delta\mathbf{h}_j$ are fixed, this defines an inverse problem for the hypocentroid $\bar{\mathbf{h}}$ and travel-time correction vector $\boldsymbol{\gamma}$. We see that the problem displays a complete ambiguity between $\mathcal{F}(\bar{\mathbf{h}}; \mathbf{m}^{\text{ref}})$ and $\boldsymbol{\gamma}$ and, thus, between $\bar{\mathbf{h}}$ itself and $\boldsymbol{\gamma}$. That is, given a potential solution $(\bar{\mathbf{h}}_1, \boldsymbol{\gamma}_1)$,

any other hypocentroid $\bar{\mathbf{h}}_2$ will be an equally good solution by setting its associated correction vector to

$$\boldsymbol{\gamma}_2 = \boldsymbol{\gamma}_1 + \mathcal{F}(\bar{\mathbf{h}}_1; \mathbf{m}^{\text{ref}}) - \mathcal{F}(\bar{\mathbf{h}}_2; \mathbf{m}^{\text{ref}}). \tag{12}$$

The complete ambiguity between $\bar{\mathbf{h}}$ and $\boldsymbol{\gamma}$ occurs only in the limit of zero cluster dimension ($\Delta\mathbf{h}_j \to 0$) since linearization of the F_j is exact only in this limit. For clusters of finite dimension, the data will contain some information to constrain the hypocentroid, as a result of nonlinearity, but it will generally be weak. With $\boldsymbol{\gamma}$ unconstrained, only the cluster vectors are well determined in the multiple-event location problem.

Therefore, absolute event locations will be well determined only if prior constraints on the travel-time corrections or on one or more of the event hypocenters is available. Given that non-seismic ground-truth event information is rarely available, a more common source of prior information on event locations is a local seismic network, which can provide an accurate location for one or more of the events in a cluster if the network is sufficiently well distributed. However, good local networks are not available in many regions, which motivated Bondár *et al.* (2008) to develop reciprocal cluster analysis. The RCA method can use a small number of local stations (as few as one) to determine the hypocentroid of a cluster. Exploiting the source-receiver reciprocity of travel times, the method treats a cluster of events as a seismic network to "relocate" local stations; the resulting station mislocations are then used to correct the cluster hypocentroid. Thus, the HDC-RCA hybrid method is a two-step process: (1) application of the traditional HDC method to regional and teleseismic arrival-time data to determine cluster vectors and a preliminary estimate of the cluster hypocentroid. followed by (2) application of RCA to data from local stations to refine (shift) the hypocentroid, with the cluster vectors unchanged.

3.1.2 Extensions

This project is extending multiple-event location methodology in three key respects. The first is to use all arrival-time data — including local, regional and teleseismic — in a unified analysis. In principle, the HDC-RCA method will then be invoked when the regional/teleseismic travel-time corrections are unconstrained and local corrections are set to zero. Solving the multiple-event location inverse problem in a single step is expected to have algorithmic advantages as well as facilitate uncertainty analysis.

The second extension to multiple-event location methodology we are developing in this project pertains to the numerical algorithm used to solve the problem. We are developing a general algorithm based on grid-search and nonlinear conjugate gradients techniques, avoiding matrix inversion or diagonalization. In addition to scaling better to large data sets, these numerical techniques allow the use of non-Gaussian distributions for observational (pick) errors, which previous work has shown to be an effective device for mitigating the effects of outliers in the observed data (e.g. Billings *et al.*, 1994; Kennett, 2006; Rodi, 2006).

The third extension is to allow prior information on travel-time corrections in the form of prior variances on the corrections and prior covariances between them. The variances and covariances can be generated from assumed geostatistical parameters of velocity heterogeneity in the Earth using the travel-time covariance modeling technique developed by Rodi and Myers (2013). The traditional practice of allowing the corrections to be unconstrained effectively assigns them infinite

prior variance. The motivation for this extension is the hope that realistic, finite variances will preserve useful information about absolute event locations.

In conjunction with this third extension, we are attempting to introduce event-location dependence into travel-time corrections. As defined above, the travel-time corrections for any given event can be expressed as eq. (4) with

$$\boldsymbol{\gamma} = \mathcal{F}(\mathbf{h}^{\mathsf{ref}}; \mathbf{m}) - \mathcal{F}(\mathbf{h}^{\mathsf{ref}}; \mathbf{m}^{\mathsf{ref}}) \tag{13}$$

where $\mathcal{F}$ is the master forward function introduced above (calculating travel times for the unique station/phase-types in the data set) and $\mathbf{h}^{\mathsf{ref}}$ is, by assumption, any hypocenter in or near the cluster (e.g. the hypocentroid). We can introduce a limited dependence of $\mathbf{c}_j$ on $\mathbf{h}_j$ as follows. Let $\mathbf{h}_k^{\mathsf{ref}}$, $k = 1, \ldots, K$, be a set of reference hypocenters and define a set of master correction vectors as

$$\boldsymbol{\gamma}_k = \mathcal{F}(\mathbf{h}_k^{\mathsf{ref}}; \mathbf{m}) - \mathcal{F}(\mathbf{h}_k^{\mathsf{ref}}; \mathbf{m}^{\mathsf{ref}}), \quad k = 1, \ldots, K. \tag{14}$$

For example, the $\mathbf{h}_k^{\mathsf{ref}}$ could be the nodes of a regular hypocenter grid which, if it contained only one point, would revert to the event-independence assumption. Now let $\boldsymbol{\gamma}$ be the concatenation of the $\boldsymbol{\gamma}_k$ into a single vector:

$$\boldsymbol{\gamma} = \begin{pmatrix} \boldsymbol{\gamma}_1 \\ \vdots \\ \boldsymbol{\gamma}_K \end{pmatrix}. \tag{15}$$

Then, $\mathbf{c}_j$ can still be defined by eq. (4) by redefining the matrices $\mathbf{S}_j$, each now containing K times as many columns, to perform spatial interpolation with respect to the $\mathbf{h}_k^{\mathsf{ref}}$ in addition to station/phase selection. Owing to interpolation, $\mathbf{S}_j$ will depend on $\mathbf{h}_j$.

We are implementing these extensions as an extended version of MIT's event-location software GMEL (Rodi, 2006). At this time, our implementation is restricted to the special case of a single reference event and master correction vector ($K = 1$), corresponding to traditional multiple-event location methods like HDC.

3.2 Bayesian Framework

Our new multiple-event location method is based on a Bayesian framework in which *prior* probability distributions on the pick errors ($\mathbf{e}_j$) and problem unknowns ($\mathbf{h}_j$ and $\boldsymbol{\gamma}$) are specified, and a solution of the problem is embodied in a *posterior* joint probability distribution on the unknowns or specific properties thereof. We have implemented the Bayesian approach under the following assumptions about prior probability distributions:

- The pick errors (elements of the $\mathbf{e}_j$) are mutually independent, zero-mean random variables, each having a specified probability distribution, which may be non-Gaussian.
- The master travel-time correction vector $\boldsymbol{\gamma}$ is jointly Gaussian with zero mean and a specified variance (variance-covariance) matrix $\boldsymbol{\Gamma}^{\mathsf{pri}}$.
- The event hypocenter vectors $\mathbf{h}_j$ are mutually independent and Gaussian, with each having a specified mean $\mathbf{h}_j^{\mathsf{pri}}$ and 4×4 variance matrix $\mathbf{H}_j^{\mathsf{pri}}$.

Our multiple-event location algorithm finds the MAP (maximum *a posteriori*) estimates of the event locations and travel-time corrections, defined to maximize their joint posterior probability distribution. Equivalently, the MAP estimates *minimize* the negative logarithm of the posterior distribution, which defines a cost function we denote as Ψ. Under the assumptions above, the cost function (omitting a constant term) is given by

$$\Psi(\mathbf{h}_1, \ldots, \mathbf{h}_J, \boldsymbol{\gamma}; \mathbf{t}_1, \ldots, \mathbf{t}_J) = \\ \sum_{j=1}^{J} \Phi_j(\mathbf{h}_j, \boldsymbol{\gamma}; \mathbf{t}_j) + \frac{1}{2}\sum_{j=1}^{J}(\mathbf{h}_j - \mathbf{h}_j^{\mathsf{pri}})^T \left(\mathbf{H}_j^{\mathsf{pri}}\right)^{-1}(\mathbf{h}_j - \mathbf{h}_j^{\mathsf{pri}}) + \frac{1}{2}\boldsymbol{\gamma}^T \left(\boldsymbol{\Gamma}^{\mathsf{pri}}\right)^{-1}\boldsymbol{\gamma} \qquad (16)$$

where Φ_j denotes a data misfit function for the jth event implied by the assumed prior probability distribution for pick errors. We assume pick errors have a generalized Gaussian distribution (e.g. Billings *et al.*, 1994) of some order $p \geq 1$, in which case the data misfit functions are given by

$$\Phi_j(\mathbf{h}_j, \boldsymbol{\gamma}; \mathbf{t}_j) = \frac{1}{p}\sum_{i=1}^{N_j} \left| t_{ij} - F_{ij}(\mathbf{h}_j; \mathbf{m}^{\mathsf{ref}}) - \mathbf{s}_{ij}^T \boldsymbol{\gamma} \right|^p / \sigma_{ij}^p \qquad (17)$$

where N_j is the number of data in $\mathbf{t}_j$; t_{ij} is the ith element of $\mathbf{t}_j$; F_{ij} is the forward modeling function for t_{ij}, as extracted from F_j; the vector $\mathbf{s}_{ij}$ (which in general depends on $\mathbf{h}_j$) is the ith column of $\mathbf{S}_j^T$, the transposed selection/interpolation matrix; and σ_{ij} is an assigned standard pick error. The generalized Gaussian distribution becomes Gaussian, and Φ_j becomes a quadratic function of the data residuals, when $p = 2$.

3.3 Travel-Time Covariances

Rodi and Myers (2013) developed a method for calculating the variance matrix of travel-time prediction errors as determined by geostatistical parameters characterizing errors in the velocity model used for travel-time prediction. This project is applying this method to generate the prior variance matrix $\boldsymbol{\Gamma}^{\mathsf{pri}}$.

The Rodi-Myers method assumes a linear relationship between model velocity (or slowness) error and travel-time errors. We thus linearize eq. (14) to obtain

$$\boldsymbol{\gamma}_k \approx \mathbf{A}_k(\mathbf{m} - \mathbf{m}^{\mathsf{ref}}), \quad k = 1, \ldots, K \qquad (18)$$

where $\mathbf{A}_k$ is the Jacobian of $\mathcal{F}(\mathbf{h}_k^{\mathsf{ref}}; \mathbf{m})$ with respect to $\mathbf{m}$ evaluated at $\mathbf{m} = \mathbf{m}^{\mathsf{ref}}$. The elements of $\mathbf{A}$ are sensitivities to the velocity model parameters calculated from the geometrical ray, for the appropriate station/phase, connecting $\mathbf{h}_k^{\mathsf{ref}}$ to the station location. Concatenating the Jacobians as

$$\mathbf{A} = \begin{pmatrix} \mathbf{A}_1 \\ \vdots \\ \mathbf{A}_K \end{pmatrix} \qquad (19)$$

and recalling (15), we can write (18) more concisely as

$$\boldsymbol{\gamma} \approx \mathbf{A}(\mathbf{m} - \mathbf{m}^{\mathsf{ref}}). \qquad (20)$$

The method of Rodi and Myers (2013) assumes that $\mathbf{m}$, the velocity model corresponding to the real Earth, is a Gaussian random variable with known mean and variance; here we will take

$$\mathrm{E}[\mathbf{m}] = \mathbf{m}^{\mathsf{ref}} \tag{21}$$

$$\mathrm{Var}[\mathbf{m}] = \mathbf{C} \tag{22}$$

where $\mathbf{C}$ is a given variance matrix. Eqs. (20)–(22) imply that $\boldsymbol{\gamma}$ is Gaussian with zero mean and variance matrix given by

$$\boldsymbol{\Gamma}^{\mathsf{pri}} = \mathbf{A}\mathbf{C}\mathbf{A}^T. \tag{23}$$

The Rodi-Myers method specifies the model variance indirectly in terms of its inverse, $\mathbf{C}^{-1}$, which is parameterized with geostatistical parameters comprising a velocity variance and spatial correlation lengths in the horizontal and vertical directions. The method calculates the ℓth column of $\boldsymbol{\Gamma}^{\mathsf{pri}}$ as $\mathbf{A}\mathbf{u}$, with $\mathbf{u}$ obtained as the solution to the linear system

$$\mathbf{C}^{-1}\mathbf{u} = \mathbf{a}_\ell \tag{24}$$

where $\mathbf{a}_\ell$ is the ℓth column of $\mathbf{A}^T$, i.e. the model sensitivities corresponding to the ℓth ray. For teleseismic rays, $\mathbf{a}_\ell$ can have many non-zero entries (compared to local and regional rays), requiring much computational effort to solve the linear system (24). This project devoted significant effort to speeding up this calculation by avoiding calculation of elements of $\mathbf{u}$ which are predictably small, i.e. those corresponding to velocity model nodes far from the ray.

3.4 Minimization Algorithm

We have enhanced GMEL to perform the minimization of Ψ in eq. (16) with a hybrid method that combines nonlinear conjugate gradients (NLCG) to perform minimization with respect to $\boldsymbol{\gamma}$ and grid search to perform minimization with respect to the $\mathbf{h}_j$. To be specific, define a reduced cost function, $\bar{\Psi}$, as

$$\bar{\Psi}(\boldsymbol{\gamma}; \mathbf{t}_1, \ldots, \mathbf{t}_J) = \min_{\mathbf{h}_1, \ldots, \mathbf{h}_J} \Psi(\mathbf{h}_1, \ldots, \mathbf{h}_J, \boldsymbol{\gamma}; \mathbf{t}_1, \ldots, \mathbf{t}_J). \tag{25}$$

Since $\bar{\Psi}$ is minimum with respect to the $\mathbf{h}_j$ for any fixed $\boldsymbol{\gamma}$, minimization of $\bar{\Psi}$ with respect to $\boldsymbol{\gamma}$ achieves joint minimization of Ψ with respect to the $\mathbf{h}_j$ and $\boldsymbol{\gamma}$. Further, we can see from eq. (16) that, with $\boldsymbol{\gamma}$ fixed, the task of minimizing Ψ with respect to hypocenters decouples across events. GMEL performs this task by applying grid search to each event hypocenter in turn.

NLCG is applied to the minimization of $\bar{\Psi}$ with respect to $\boldsymbol{\gamma}$. This method is well documented in the optimization literature (e.g. Kelley, 1999) and we focus here on our implementation of the method. NLCG is an iterative method in which the ℓth solution iterate is updated according to (initializing with $\boldsymbol{\gamma}^0 = 0$)

$$\boldsymbol{\gamma}^{\ell+1} = \boldsymbol{\gamma}^\ell + \alpha^\ell \, \mathbf{p}^\ell \tag{26}$$

where the vector $\mathbf{p}^\ell$ denotes a search direction and the scalar α^ℓ a step-length in that direction. The search direction is generated recursively as

$$\mathbf{p}^\ell = \mathbf{P}\mathbf{g}^\ell + \beta^\ell \, \mathbf{p}^{\ell-1} \tag{27}$$

where $\mathbf{g}^\ell$ is the gradient of $\bar{\Psi}$ with respect to $\boldsymbol{\gamma}$, evaluated at $\boldsymbol{\gamma}^\ell$; $\mathbf{P}$ is a symmetric, positive definite preconditioning matrix; and β^ℓ is a memory factor. Eq. (16) and the stationarity of Ψ with respect to the hypocenters imply that

$$\begin{aligned}\mathbf{g}^\ell &\equiv \nabla\bar{\Psi}(\boldsymbol{\gamma}^\ell; \mathbf{t}_1, \ldots, \mathbf{t}_J) \\ &= \sum_{j=1}^{J} \nabla\Phi_j(\mathbf{h}_j^\ell, \boldsymbol{\gamma}^\ell; \mathbf{t}_j) + \left(\boldsymbol{\Gamma}^{\mathsf{pri}}\right)^{-1}\boldsymbol{\gamma}^\ell. \end{aligned} \tag{28}$$

Here ∇ denotes gradient with respect to $\boldsymbol{\gamma}$, and the $\mathbf{h}_j^\ell$ denote the hypocenters that minimize Ψ for the current $\boldsymbol{\gamma}$, i.e.

$$\bar{\Psi}(\boldsymbol{\gamma}^\ell; \mathbf{t}_1, \ldots, \mathbf{t}_J) = \Psi(\mathbf{h}_1^\ell, \ldots, \mathbf{h}_J^\ell, \boldsymbol{\gamma}^\ell; \mathbf{t}_1, \ldots, \mathbf{t}_J). \tag{29}$$

A crucial feature of our implementation of NLCG in GMEL is the choice of the preconditioner, which we set to the prior variance on $\boldsymbol{\gamma}$:

$$\mathbf{P} = \boldsymbol{\Gamma}^{\mathsf{pri}}. \tag{30}$$

By doing so, the calculations can be coded to avoid the use of the inverse of $\boldsymbol{\Gamma}^{\mathsf{pri}}$; only operations with $\boldsymbol{\Gamma}^{\mathsf{pri}}$ itself are needed. Looking at (28), we see this to be the case for the calculation of the preconditioned gradient, $\boldsymbol{\Gamma}^{\mathsf{pri}}\,\mathbf{g}^\ell$, which is used in eq. (27) as well as in the formula for β^ℓ (not shown here). Additionally, our implementation carries the quantities

$$\boldsymbol{\eta}^\ell \equiv (\boldsymbol{\Gamma}^{\mathsf{pri}})^{-1}\boldsymbol{\gamma}^\ell \tag{31}$$

$$\mathbf{q}^\ell \equiv (\boldsymbol{\Gamma}^{\mathsf{pri}})^{-1}\mathbf{p}^\ell \tag{32}$$

using the recursions

$$\boldsymbol{\eta}^{\ell+1} = \boldsymbol{\eta}^\ell + \alpha^\ell\,\mathbf{q}^\ell \tag{33}$$

$$\mathbf{q}^\ell = \mathbf{g}^\ell + \beta^\ell\,\mathbf{q}^{\ell-1} \tag{34}$$

which also avoid operation with $(\boldsymbol{\Gamma}^{\mathsf{pri}})^{-1}$. The last term of the cost function in eq. (16) can then be calculated using

$$(\boldsymbol{\gamma}^\ell)^T\left(\boldsymbol{\Gamma}^{\mathsf{pri}}\right)^{-1}\boldsymbol{\gamma}^\ell = (\boldsymbol{\gamma}^\ell)^T\boldsymbol{\eta}^\ell. \tag{35}$$

Estimation of Pick-Error Variances

The variance of each pick error (e_{ij}) is proportional to the square of its standard error:

$$\mathrm{Var}[e_{ij}] \propto \sigma_{ij}^2 \tag{36}$$

where the proportionality factor depends on the order of the generalized Gaussian distribution and is one for the Gaussian case ($p=2$). GMEL allows the σ_{ij} to be unknowns in the multiple-event location problem in addition to $\boldsymbol{\gamma}$ and the $\mathbf{h}_j$. As this capability is used in this project, each station/phase-type pair is assigned a standard pick error ν_k, common to all events, such that

$$\sigma_{ij} = \nu_{K(i,j)} \tag{37}$$

where the function K reports the station/phase-type combination for an individual datum. Prior to updating $\boldsymbol{\gamma}$ at each step of the NLCG iteration, the standard errors are updated with

$$\left(\nu_k\right)^p = \frac{1}{N_k} \sum_{ij:K(i,j)=k} \left| t_{ij} - F_{ij}(\mathbf{h}_j; \mathbf{m}^{\mathsf{ref}}) - \mathbf{s}_{ij}^T \boldsymbol{\gamma} \right|^p \tag{38}$$

where N_k denotes the number of data for the kth station/phase combination. This updating formula is derived as the maximum-likelihood estimate of ν_k, but its value is clipped to obey prescribed upper and lower bounds. Since the arrival-time residuals depend on the event hypocenters, the grid searches for the $\mathbf{h}_j$ and the resetting of the ν_k are repeated until a convergence is reached, creating an inner loop within the NLCG loop.

3.5 Location Uncertainty Algorithm

In the first year of the project we formulated an approach to the calculation of hypocenter uncertainty in the multiple-event location problem, although we have not yet implemented it in GMEL. The approach is similar to that of Rodi (2008) but promises to be more practical.

The primary quantity of interest is the uncertainty in the 4-component hypocenter vector $\mathbf{h}_j$ for any given j. In the framework of Bayesian inference, this is described by the *marginal* posterior probability distribution of $\mathbf{h}_j$, marginalized with respect to the remaining hypocenter vectors, $\mathbf{h}_{j'}$, $j' \neq j$, and the travel-time correction vector $\boldsymbol{\gamma}$. This marginal distribution accounts for the uncertainty in $\mathbf{h}_j$ induced by trade-offs with all these other parameters, in addition to that induced by pick errors in its own observations $\mathbf{t}_j$. Rodi (2008) considered multiple-event location uncertainty in a fully nonlinear, non-Gaussian ($p \neq 2$) framework, leading to a computationally intensive algorithm for computing location confidence regions. A much more efficient algorithm resulted with the use of Gaussian approximations to posterior distributions. The uncertainty approach we have formulated for this project makes use of such approximations.

The *joint* posterior distribution of all the unknown parameters in the multiple-event location problem is given by

$$p(\mathbf{h}_1, \ldots, \mathbf{h}_J, \boldsymbol{\gamma} \,|\, \mathbf{t}_1, \ldots, \mathbf{t}_J) = K_0 \, \exp\left\{ -\Psi(\mathbf{h}_1, \ldots, \mathbf{h}_J, \boldsymbol{\gamma}; \mathbf{t}_1, \ldots, \mathbf{t}_J) \right\} \tag{39}$$

where K_0 is a normalizing constant. The marginal posterior on a single event location vector (say $\mathbf{h}_1$), denoted $p(\mathbf{h}_1 \mid \mathbf{t}_1, \ldots, \mathbf{t}_J)$, is obtained by integrating this joint posterior over $\mathbf{h}_2$, …, $\mathbf{h}_J$ and $\boldsymbol{\gamma}$. Given the nonlinearity of the forward problem and the possible assumption of non-Gaussian pick errors, the necessary integration cannot be done analytically or, given the large number of marginal parameters, is not amenable to numerical quadrature. An alternative is to use sampling techniques (e.g. Markov chain Monte Carlo, or MCMC) to generate an ensemble from $p(\mathbf{h}_1 \mid \mathbf{t}_1, \ldots, \mathbf{t}_J)$, as is done by the BayesLoc multiple-event location algorithm (Myers *et al.*, 2007, 2009). However, sampling techniques can be computationally intensive for large problems. A more direct approach commonly taken in nonlinear inverse problems, suitable for the case of Gaussian pick errors, is to perform uncertainty analysis under a linear approximation to the forward modeling functions, where the linearization is done around the MAP solution. That is, the forward functions are approximated as

$$F_j(\mathbf{h}_j; \mathbf{m}^{\mathsf{ref}}) \approx F_j(\mathbf{h}_j^{\mathsf{MAP}}; \mathbf{m}^{\mathsf{ref}}) + \mathbf{B}_j \left(\mathbf{h}_j - \mathbf{h}_j^{\mathsf{MAP}} \right) \tag{40}$$

where $\mathbf{B}_j$ is the Jacobian of F_j with respect to $\mathbf{h}_j$ evaluated at the MAP estimate. Under this approximation, the joint posterior distribution of the $\mathbf{h}_j$ and $\boldsymbol{\gamma}$ is Gaussian, as is the marginal posterior of $\mathbf{h}_1$. The uncertainty in $\mathbf{h}_1$ is thus fully characterized by the variance of $p(\mathbf{h}_1 \,|\, \mathbf{t}_1, \ldots, \mathbf{t}_J)$ (the posterior variance matrix), which is a partition of the joint posterior variance matrix of all the unknown parameters. Unfortunately, while the *inverse* of the joint posterior variance matrix has a simple, analytic expression, the joint variance matrix itself, or a partition of it, must be evaluated numerically with calculations performed over the full set of unknowns.

To avoid the inversion of large matrices, as well as relax the requirement of Gaussian pick errors, we have formulated a different approach to calculating an approximation to the posterior variances matrix of a hypocenter. It makes two related approximations. First, we approximate the marginal posterior distribution of $\mathbf{h}_1$ by replacing integration with minimization, i.e.

$$p(\mathbf{h}_1 \,|\, \mathbf{t}_1, \ldots, \mathbf{t}_J) \approx K_1 \, \exp\big\{ -\Psi_1(\mathbf{h}_1; \mathbf{t}_1, \ldots, \mathbf{t}_J)\big\} \tag{41}$$

where K_1 is another normalizing constant and Ψ_1 is the reduced cost function obtained by minimizing Ψ with respect to all parameters except $\mathbf{h}_1$:

$$\Psi_1(\mathbf{h}_1; \mathbf{t}_1, \ldots, \mathbf{t}_J) = \min_{\mathbf{h}_2, \ldots, \mathbf{h}_J, \boldsymbol{\gamma}} \Psi(\mathbf{h}_1, \ldots, \mathbf{h}_J, \boldsymbol{\gamma}; \mathbf{t}_1, \ldots, \mathbf{t}_J). \tag{42}$$

We note that this approximation is exact just in case the joint posterior is Gaussian. Rodi (2008) attempted to sample this approximate posterior probability distribution on a grid in $\mathbf{h}_1$ space, which turned out to be very computationally intensive since the minimization in eq. (42) is performed for each point of the sampling grid. To avoid this, we invoke a second approximation, that the marginal posterior distribution of $\mathbf{h}_1$ is Gaussian or, equivalently, the reduced cost function Ψ_1 is quadratic, taking the form

$$\Psi_1(\mathbf{h}_1; \mathbf{t}_1, \ldots, \mathbf{t}_J) \approx \frac{1}{2}(\mathbf{h}_1 - \mathbf{h}_1^{\mathsf{MAP}})^T \big(\mathbf{H}_1^{\mathsf{pos}}\big)^{-1} (\mathbf{h}_1 - \mathbf{h}_1^{\mathsf{MAP}}). \tag{43}$$

This takes the posterior mean of $\mathbf{h}_1$ to be its MAP estimate found by minimizing Ψ with respect to all the unknowns. The problem remains to calculate the posterior variance matrix implied by this approximation, $\mathbf{H}_1^{\mathsf{pos}}$.

We have formulated a perturbation technique to estimate $\mathbf{H}_1^{\mathsf{pos}}$, which proceeds as follows. Let Ψ' denote the cost function defined by augmenting Ψ as

$$\begin{aligned}\Psi'(\mathbf{h}_1, \ldots, \mathbf{h}_J; \mathbf{t}_1, \ldots, \mathbf{t}_J) = \Psi(\mathbf{h}_1, \ldots, \mathbf{h}_J; \mathbf{t}_1, \ldots, \mathbf{t}_J) \\ + \frac{1}{2}(\mathbf{h}_1 - \mathbf{h}_1^{\mathsf{MAP}} - \mathbf{a})^T \mathbf{H}_0^{-1} (\mathbf{h}_1 - \mathbf{h}_1^{\mathsf{MAP}} - \mathbf{a}).\end{aligned} \tag{44}$$

The added term plays the role of additional, independent prior information on $\mathbf{h}_1$ in the form of a Gaussian distribution with mean $(\mathbf{h}_1^{\mathsf{MAP}} + \mathbf{a})$ and variance $\mathbf{H}_0$. Owing to this addition, the hypocenters and correction vector minimizing Ψ' will be perturbed from the MAP values found to minimize Ψ.

It is easy to show that the reduced cost function Ψ_1' corresponding to Ψ' is augmented similarly to Ψ', that is

$$\begin{aligned}\Psi_1'(\mathbf{h}_1; \mathbf{t}_1, \ldots, \mathbf{t}_J) = \Psi_1(\mathbf{h}_1; \mathbf{t}_1, \ldots, \mathbf{t}_J) \\ + \frac{1}{2}(\mathbf{h}_1 - \mathbf{h}_1^{\mathsf{MAP}} - \mathbf{a})^T \mathbf{H}_0^{-1} (\mathbf{h}_1 - \mathbf{h}_1^{\mathsf{MAP}} - \mathbf{a}).\end{aligned} \tag{45}$$

The perturbed MAP estimate of $\mathbf{h}_1$ minimizes Ψ_1' and, therefore, makes the gradient of Ψ_1' equal to zero. Using the quadratic approximation (43), the gradient is given by

$$\nabla\Psi_1' = \left(\mathbf{H}_1^{\mathsf{pos}}\right)^{-1}\mathbf{x} + \mathbf{H}_0^{-1}(\mathbf{x}-\mathbf{a}) \tag{46}$$

where $\mathbf{x}$ denotes the difference between $\mathbf{h}_1$ and its unperturbed MAP estimate:

$$\mathbf{x} = \mathbf{h}_1 - \mathbf{h}_1^{\mathsf{MAP}}. \tag{47}$$

Eq. (46) implies that the hypocenter perturbation minimizing the augmented cost function satisfies

$$\mathbf{x} = \mathbf{H}_1^{\mathsf{pos}}\,\mathbf{H}_0^{-1}(\mathbf{a}-\mathbf{x}). \tag{48}$$

Suppose now we solve the perturbed multiple-event location problem for several values of $\mathbf{a}$, denoted $\mathbf{a}_\ell$ for $\ell = 1, \ldots, L$, yielding MAP perturbations $\mathbf{x}_\ell$ which satisfy

$$\mathbf{x}_\ell = \mathbf{H}_1^{\mathsf{pos}}\,\mathbf{H}_0^{-1}(\mathbf{a}_\ell - \mathbf{x}_\ell) \tag{49}$$

and thus

$$\mathbf{x}_\ell(\mathbf{a}_\ell - \mathbf{x}_\ell)^T = \mathbf{H}_1^{\mathsf{pos}}\,\mathbf{H}_0^{-1}(\mathbf{a}_\ell - \mathbf{x}_\ell)(\mathbf{a}_\ell - \mathbf{x}_\ell)^T. \tag{50}$$

Summing this equation over ℓ we obtain

$$\mathbf{N} = \mathbf{H}_1^{\mathsf{pos}}\,\mathbf{H}_0^{-1}\mathbf{M} \tag{51}$$

where

$$\mathbf{M} = \sum_{\ell=1}^{L}(\mathbf{a}_\ell - \mathbf{x}_\ell)(\mathbf{a}_\ell - \mathbf{x}_\ell)^T \tag{52}$$

$$\mathbf{N} = \sum_{\ell=1}^{L}\mathbf{x}_\ell(\mathbf{a}_\ell - \mathbf{x}_\ell)^T. \tag{53}$$

If L is sufficiently large (at least 4) and the vectors $\mathbf{a}_\ell$ sufficiently diverse, the symmetric matrix $\mathbf{M}$ will be positive definite and we can write the desired posterior variance matrix of $\mathbf{h}_1$ as

$$\mathbf{H}_1^{\mathsf{pos}} = \mathbf{N}\mathbf{M}^{-1}\mathbf{H}_0. \tag{54}$$

Our location uncertainty algorithm thus entails solving four or more perturbed multiple-event location problems to obtain the posterior variance matrix for each hypocenter, using the formula (54). To force symmetry on $\mathbf{H}_1^{\mathsf{pos}}$ we can average the matrix resulting from (54) with its transpose. Appropriate choices for the $\mathbf{a}_\ell$ and $\mathbf{H}_0$ will be addressed as the method is implemented in GMEL. If the $\mathbf{a}_\ell$ are not too large, the computational effort to solve the perturbed problems will presumably require much less than for the original (unperturbed) multiple-event location problem.

It is important to note that while this approach to location uncertainty relies on Gaussian approximations to posterior distributions, it does not explicitly assume that prior distributions are Gaussian. Thus, a non-Gaussian distribution for pick errors will still be allowed. The approximate posterior we calculate will be valid to the extent that the pooling of non-Gaussian information results in approximate Gaussian posteriors on the event hypocenters as a consequence of the central limit theorem.

4 RESULTS AND DISCUSSION

To date we have applied our new multiple-event location method to arrival-time data for two event clusters included in the IASPEI Reference Event List (REL) to demonstrate and test our approach. The first is the Rogun earthquake cluster in Tajikistan. The IASPEI REL results for this cluster were obtained with the HDC-RCA method and discussed by Bonda´r *et al.* (2008). The second cluster comprises nuclear explosions in the Pahute Mesa area of the Nevada Test Site. The IASPEI REL reports the GT0 location information for these events, allowing us to assess absolute errors in our multiple-event location solutions. Table 1 lists event and data counts for the two clusters.

The results shown here for both clusters were obtained using only first-arrival P-wave times and, since these data poorly constrain event focal depth, with event depths fixed to their catalog values. In all but one example, the AK135 1-D velocity model (Kennett *et al.*, 1995) was used as the reference model for travel-time calculation.

4.1 Rogun Cluster Results

Fig. 1 compares two GMEL multiple-event location solutions for the Rogun cluster to the HDC-RCA solution reported in the IASPEI REL. Both GMEL solutions used a diagonal covariance matrix for travel-time corrections; these examples did not use a full travel-time variance-covariance matrix generated with our covariance modeling technique. Travel-time corrections for teleseismic and regional paths (P and Pn phases, respectively) were assigned a standard deviation of 20 s, effectively treating these corrections as unconstrained. The standard deviation for local corrections (Pg and Pb phases), however, were set to zero, which fixes the corrections themselves to zero.

The panel on the left of Fig. 1 shows the GMEL solution obtained with only teleseismic and regional arrivals. As expected, the difference between the GMEL and HDC-RCA epicenters consists

Table 1: Data sets for two event clusters in the IASPEI REL.

	Rogun	Pahute Mesa
Number of events	17	57
Number of stations	371	1 205
Number of arrivals	1 356	11 078
P	1 053	8 255
Pn	270	2 771
Pg/Pb	33	52

mainly of a shift of about 13 km in the cluster centroid to the south-southeast. This demonstrates the loss of absolute event location information that is incurred when unconstrained (or weakly constrained) travel-time corrections are allowed in the multiple-event location problem. The relative patterns of the GMEL and HDC-RCA epicenters, however, are similar.

The right-hand panel of Fig. 1 shows the GMEL solution obtained with arrival-time data at local stations included with the teleseismic and regional arrivals. The GMEL and HDC-RCA epicenters now agree quite well, with the median epicentral distance between the two solutions being 3.5 km. This agreement supports the premise that including teleseismic, regional and local data into a unified analysis, with appropriate constrains on travel-time corrections, emulates the two-step HDC-RCA procedure.

The GMEL solutions in Fig. 1 were obtained with AK135 as the reference velocity model for travel-time calculation. Fig. 2 shows the corresponding results when the reference model is a hybrid constructed with the crust and uppermost mantle velocities replaced with the local 1-D velocity model used by Bondár *et al.* (2008) in their RCA analysis. We see in the left-hand frame that the hypocentroid discrepancy between GMEL and HDC-RCA has doubled (to 26 km) compared to Fig. 1, reflecting the fact that the hybrid model is worse than AK135 for teleseismic travel-time prediction. Th right-hand frame of Fig. 2, however, shows better agreement between the HDC-RCA solution and GMEL solution that includes data from local stations, with the median epicentral difference now 2.6 km. This indicates that the local model used by Bondár *et al.* (2008) is better than AK135 for predicting local travel times.

4.2 Tests With Pahute Mesa Explosions

We obtained event information and arrival-time data for 57 Pahute Mesa explosions from the IASPEI REL database. The data include arrivals at local, regional and teleseismic distances. Our tests used local arrival data at only three stations in order to emulate the situation for which the HDC-RCA method was developed: when local data by themselves are insufficient to find accurate absolute locations for any of the events. After excluding most of the local data, our data set for the Pahute cluster comprised 11,078 arrivals at 1,205 stations. Three quarters of the arrival times were from teleseismic stations and only 52 were from local stations (see Table 1). The GMEL solutions were obtained using AK135 as the reference velocity model and with event depths fixed to their ground-truth values

4.2.1 Basic Tests

Our first test applied single-event location to the Pahute Mesa cluster. Single-event location occurs when all the travel-time corrections are fixed to zero, which decouples the location problem across events. The GMEL solution for the event epicenters is shown as the blue dots in Fig. 3, which also shows the mislocations from the GT0 epicenters (red circles). The comparison is displayed in two ways. The left-hand panel compares the *absolute* GMEL epicenters to their GT0 counterparts. The panel on the right compares a shifted version of the GMEL epicenters to the GT0 epicenters, where the shift was calculated so that the centroid of the GMEL epicenters matched the GT0 centroid. The resulting mislocations thus indicate the errors in the *relative* event locations, or *cluster vectors*. The median epicentral mislocation for the 57 events is 4.3 km, with a 3.4 km shift of the cluster centroid to the south accounting for much of the mislocation.

Table 2: Mislocation statistics for the epicenters of 57 Pahute Mesa explosions, displayed in Fig. 6.

Variance treatment	*Distrib. type*	*Median misloc. (km)*	*Largest misloc. (km)*	*Centroid misloc. (km)*
fixed	Gaussian	2.4	8.8	1.9
fixed	non-Gaussian	0.9	3.9	0.6
adjustable	Gaussian	2.1	4.4	1.9
adjustable	non-Gaussian	2.1	4.1	2.0

Fig. 4 compares a multiple-event solution obtained with GMEL to the GT0 epicenters. As in the Rogun example above, the travel-time corrections for the 52 local (Pg) paths were fixed to zero, while teleseismic and regional corrections were assigned 20-s standard deviation, thus emulating the HDC-RCA method. We see that, by allowing weakly constrained travel-time corrections for regional/teleseismic paths, both absolute and relative epicenter mislocations are reduced. The median mislocation in this case is 2.4 km.

Fig. 5 displays the single-event location and multiple-event location solutions shown in Figs. 3 and 4 (respectively) as polar plots of mislocation vectors. The origin of each plot represents the GT0 epicenters of the explosions (superposed) while each circle is the GMEL epicenter relative to the GT0 location, which thus shows its absolute mislocation. Displayed in this fashion, it is very clear that the multiple-event location solution (right) is significantly better than the single-event location solution. The better relative locations are evident by the more tightly clustered, less scattered, mislocation vectors.

4.2.2 Outlier Suppression

The GMEL multiple-event location solution shown in the right-hand frame of Fig. 5 displays some large mislocations (for two events in particular) which are likely due to outliers in the arrival-time data set. We thus explored the use of two techniques for mitigating the effects of outliers. One is to replace the assumed Gaussian distribution for pick errors with a longer tailed non-Gaussian distribution, which we took to be a generalized Gaussian distribution with $p = 1.25$ (compared to $p = 2$ for Gaussian). The second device for outlier suppression we considered was data re-weighting, whereby pick-error standard errors were adjusted as part of the GMEL solution using the variance estimation technique described in Section 3.4.1.

Fig. 6 compares GMEL solutions obtained with and without the use of each outlier suppression technique. (The top left-hand panel thus repeats the right panel of Fig. 5.) Table 2 reports the median and maximum epicentral mislocation for each case, as well as the mislocation of the cluster centroid for each. We see from the table and mislocation plots in Fig. 6 that both outlier suppression techniques reduce epicentral mislocations. The smallest mislocations and smallest centroid shift results with the long-tailed, non-Gaussian pick-error distribution with fixed variances

Table 3: Geostatistical parameters of velocity heterogeneity (relative to AK135) used for calculation of prior covariance matrix of travel-time corrections.

	Velocity Std. dev.	Correl. length (km) Horiz.	Vert.
Crust	10 %	300	17.5
Moho – 210 km	2 %	300	60
210 – 410 km	1 %	300	60
410 – 660 km	1 %	300	60
$>$ 660 km	0.5 %	300	120

Table 4: Mislocation statistics for GMEL results in Fig. 8, obtained with a full covariance matrix for local, regional and teleseismic travel-time corrections.

Variance treatment	*Distrib. type*	*Median misloc. (km)*	*Largest misloc. (km)*	*Centroid misloc. (km)*
fixed	Gaussian	3.0	14.1	2.5
fixed	non-Gaussian	3.0	4.7	2.8
adjustable	Gaussian	2.6	4.7	2.3
adjustable	non-Gaussian	2.2	3.8	2.0

4.2.3 Full Covariance Matrix

All the GMEL solutions presented thus far followed the HDC-RCA prescription for travel-time corrections, with large variances assigned to regional and teleseismic paths (similar to the HDC method) and zero corrections assigned to local paths (as in RCA). Further, the corrections were assumed to be uncorrelated with one another, implying the variance-covariance matrix ($\mathbf{\Gamma}^{\text{pri}}$ in Section 3) is diagonal. The next results we show used a full variance-covariance matrix for travel-time corrections, generated from a geostatistical model of the velocity difference between the real Earth and the AK135 reference model. We considered only one set of geostatistical parameters, listed in Table 3. The parameters are similar to those inferred by Rodi and Myers (2013) from travel-time observations, although our velocity variances below 210 km depth are somewhat larger. Using these parameters we calculated the variance-covariance matrix for the paths from an event location near the center of the Pahute Mesa explosion cluster to the stations in the Pahute Mesa data set. The travel-time standard deviations derived from the diagonal elements of the resulting 1205×1205 matrix are plotted as a function of event-station distance (out to 50°) in Fig. 7.

Fig. 8 shows the GMEL epicenter mislocations resulting with the use of the full variance-covariance matrix for travel-time corrections. As above, there are four cases corresponding to different treatments of pick errors. Mislocation statistics for the four cases are listed in Table 4. It is clear that the mislocations are generally larger than the previous cases which used the HDC-RCA assumptions (Fig. 6 and Table 2). The smallest mislocations now result from the use of

Table 5: Mislocation statistics for GMEL results in Fig. 9, obtained with zero variances for local travel-time corrections and a full covariance matrix for teleseismic and regional corrections.

Variance treatment	*Distrib. type*	*Median misloc. (km)*	*Largest misloc. (km)*	*Centroid misloc. (km)*
fixed	Gaussian	1.6	13.9	1.1
fixed	non-Gaussian	1.1	5.8	0.4
adjustable	Gaussian	1.7	3.9	1.4
adjustable	non-Gaussian	1.2	3.1	0.7

both outlier suppression techniques (non-Gaussian pick errors with adjustable variances), although unlike before it appears that the use of adjustable pick-error variances is the more effective of the two techniques.

Pending further analysis, we attribute the larger mislocations resulting with our travel-time covariance modeling to the somewhat large standard deviations that were calculated for local corrections: 0.8, 0.9 and 3.1 seconds at stations BGB, GLR and TNP, respectively. The arrival-time data at these stations are thus down-weighted relative to teleseismic and regional data with an accompanying loss of information about the absolute event locations.
With this explanation in mind, we reran the cases in Fig. 8 using a modified version of the full covariance matrix with local-station variances (and associated covariances) set to zero. The results are shown in Fig. 9 and summarized in Table 5. The mislocations are now comparable to those obtained with the diagonal covariance matrix shown earlier, which also used zero local corrections. The best cases seen in Table 5 are those using a non-Gaussian distribution for pick errors, which rival the best case resulting with the HDC-RCA assumptions. The use of both techniques for outlier suppression now yields a maximum mislocation of 3.1 km, the smallest value of this metric among all 12 GMEL solutions we have presented.

4.3 Database Compilation

The multiple-event location methodology we are developing is expected to have less restrictive criteria on allowable event and station geometries than previous methods. Therefore, we are assembling a database of event clusters from the International Seismological Centre's Reviewed Event Bulletin (ISC REB), which is more complete than the IASPEI REL. We began this task by downloading the current ISC REB, which spans the time frame between January 1963 and February 2012. There are readings prior to 1960, but the events are sparsely recorded and not of much use for our purposes. The bulletin is stored as year-long, downloadable files in the IASPEI Seismic Format (ISF) from 2004 to 2012. Prior to 2004, the bulletins must be retrieved through web service calls, using a script that downloads one day at a time. Dr. Reiter wrote the scripts to retrieve the bulletins and then adapted a program from Dr. Rodi to convert the results from HTML browser format to the ASCII flat files that are read by the GMEL software.

The number of events and station readings in the ISC bulletin goes up dramatically starting in the 1990s. For example, for years 1963-1989 there are 197,939 events with 12,354,668 phase readings. In the years 1990-1999 the bulletin contains 166,394 events with 10,058,285 phase readings; the years 2000-2009 contain 360,457 events (35,254,318 phases); and the 26 months in the bulletin from 2010 to 2012 have 94,666 events (11,138,496 readings). Put more simply, the ISC bulletin from the most recent 26 months contains nearly half of the events and almost the same number of phases as the bulletin from the first 27 years. The next step of database compilation is to compile expanded data sets of event clusters and their arrival picks for events which appear in the IASPEI REL, and to identify new clusters in areas of monitoring interest.

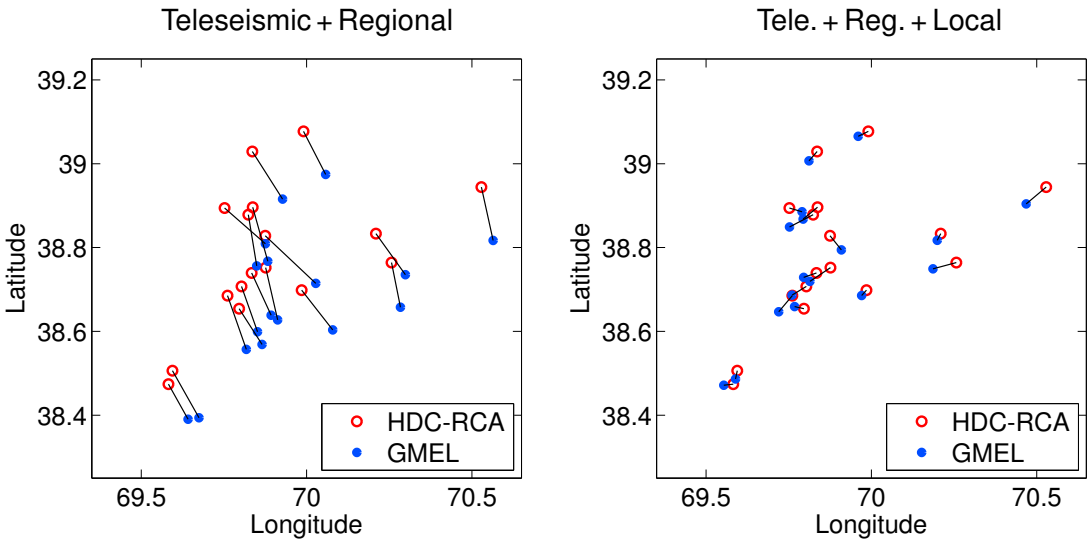

Figure 1: Two GMEL solutions for the Rogun earthquake cluster are compared to the HDC-RCA solution reported in the IASPEI REL. *Left:* Multiple-event location was applied to only teleseismic and regional data. *Right:* Local arrival times were added with their travel-time corrections fixed to zero, which emulates the HDC-RCA method. In each plot, a line connects the GMEL epicenter for each event with the corresponding HDC-RCA epicenter.

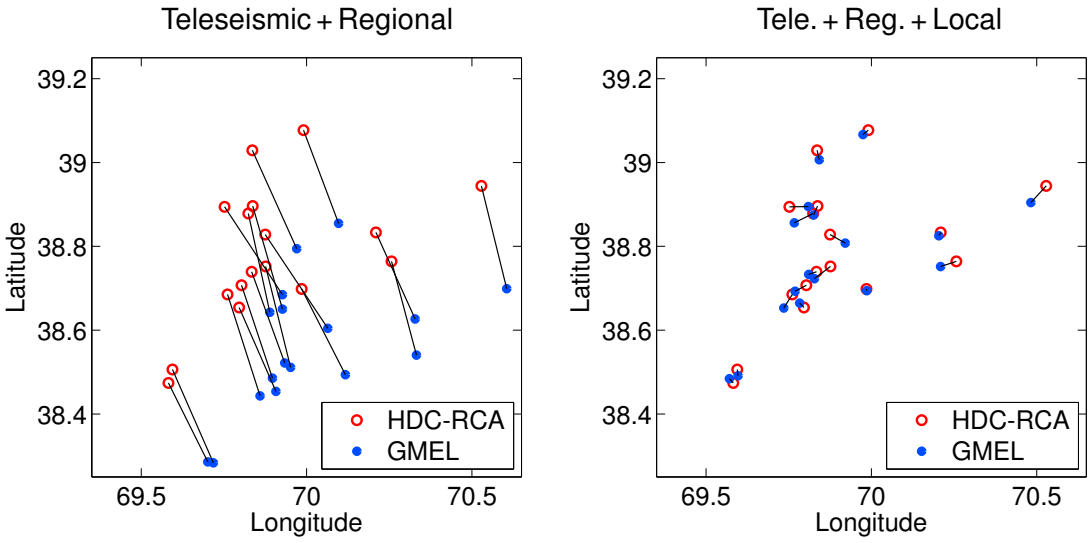

Figure 2: Same as Fig. 1 except that a hybrid velocity model incorporating the crustal model used by Bondár *et al.* (2008) was used (instead of AK135) as the reference model for travel-tine calculation.

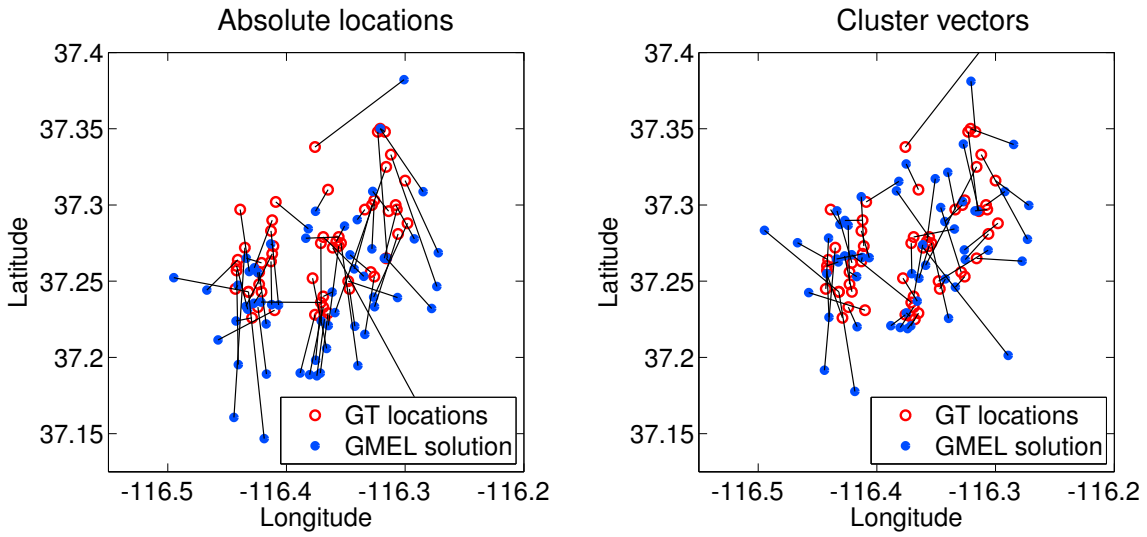

Figure 3: GMEL solution for the epicenters of 57 Pahute Mesa explosions obtained with single-event location. The GMEL epicenters are compared to the GT0 epicenters in two ways. *Left:* the *absolute* GMEL epicenters and mislocation vectors are plotted. *Right:* the GMEL epicenters are shifted to match the centroid of the GT0 epicenters, this displaying *relative* mislocations, i.e. errors in the cluster vectors.

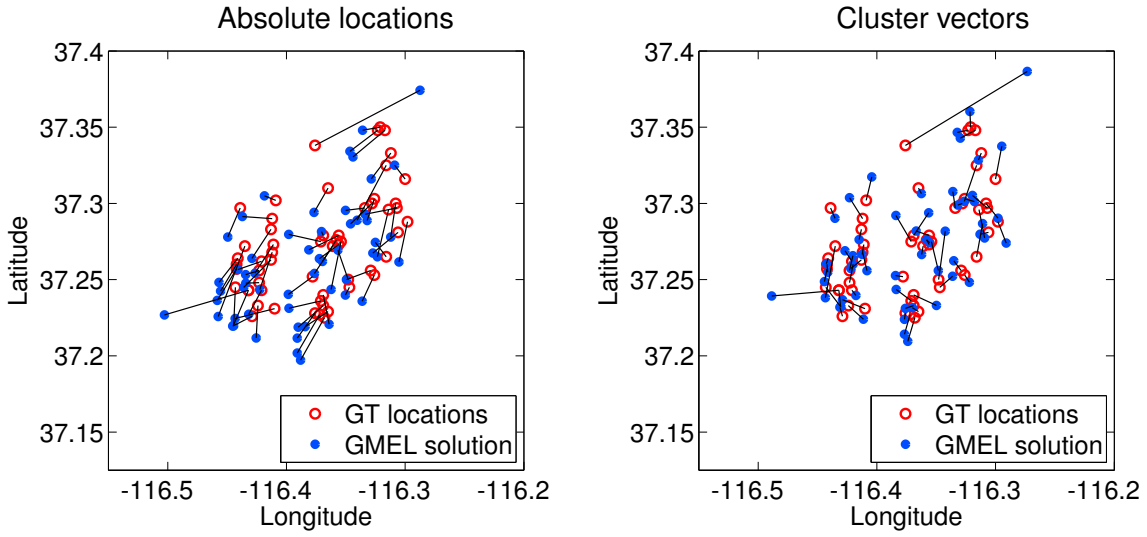

Figure 4: GMEL solution for the Pahute Mesa explosion epicenters obtained with multiple-event location. The arrival-time data set includes 52 Pg phases from three local station, whose travel-time corrections were fixed to zero to emulate the RCA procedure. The solution is displayed in the same format as Fig. 3.

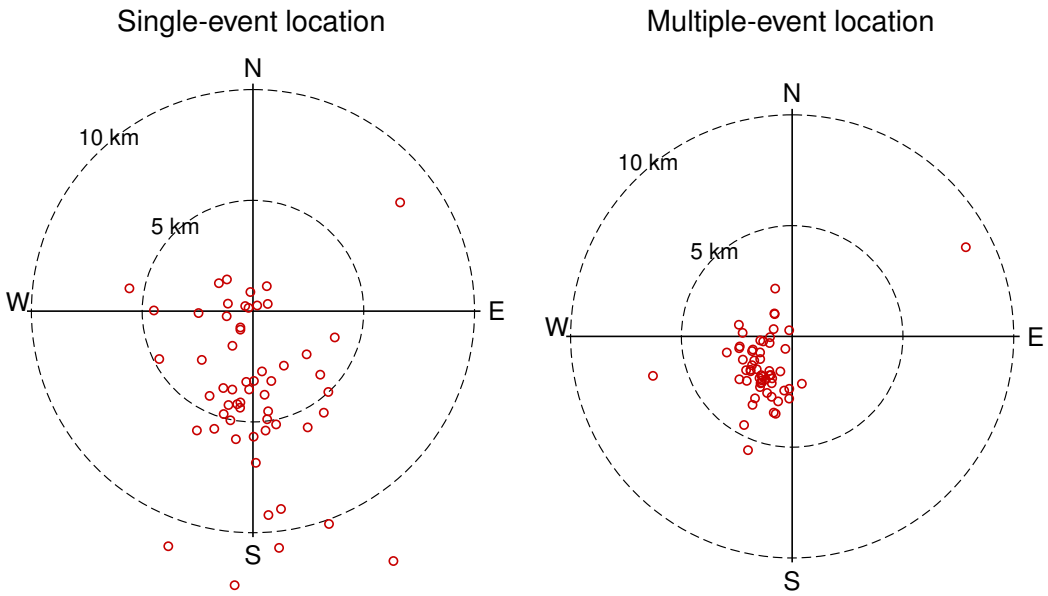

Figure 5: The GMEL solutions for the Pahute Mesa explosions in Figs. 3 (single-event location) and 4 (multiple-event location) are shown as polar plots of mislocation vectors. The origin of each plot represents the GT0 epicenters, while the dots are the mislocation vectors for the GMEL solution.

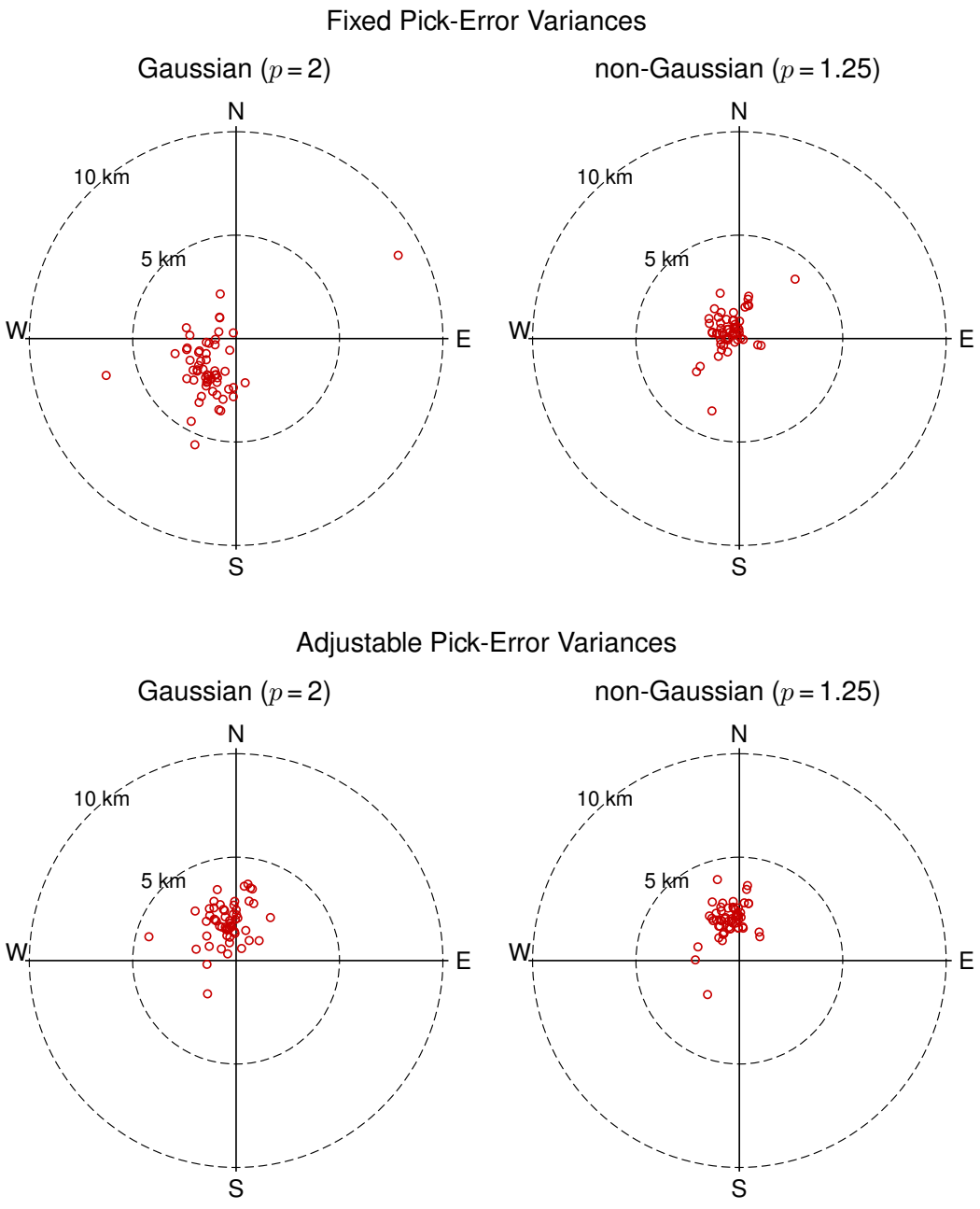

Figure 6: Mislocation vectors of GMEL solutions for the epicenters of 57 Pahute Mesa explosions for four different treatments of pick errors. *Top left:* pick errors are Gaussian ($p = 2$) with pre-assigned (fixed) variances (repeats Fig. 5 right). *Top right:* non-Gaussian ($p = 1.25$) pick errors with fixed variances. *Bottom left:* Gaussian with adjustable variances, solved for as part of the GMEL solution. *Bottom right:* non-Gaussian with adjustable variances.

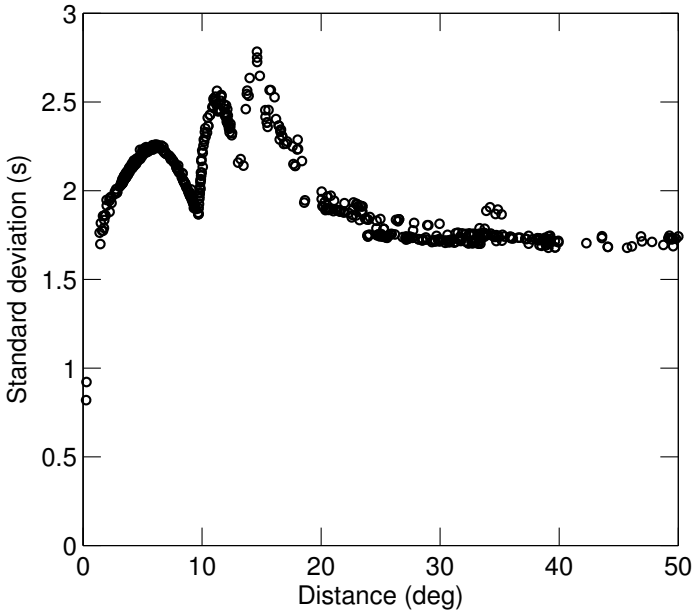

Figure 7: The first-arrival P-wave travel-time correction standard deviations for the paths in the Pahute Mesa data set are plotted as a function of event-station distance, as computed from the geostatistical parameters of velocity listed in Table 3.

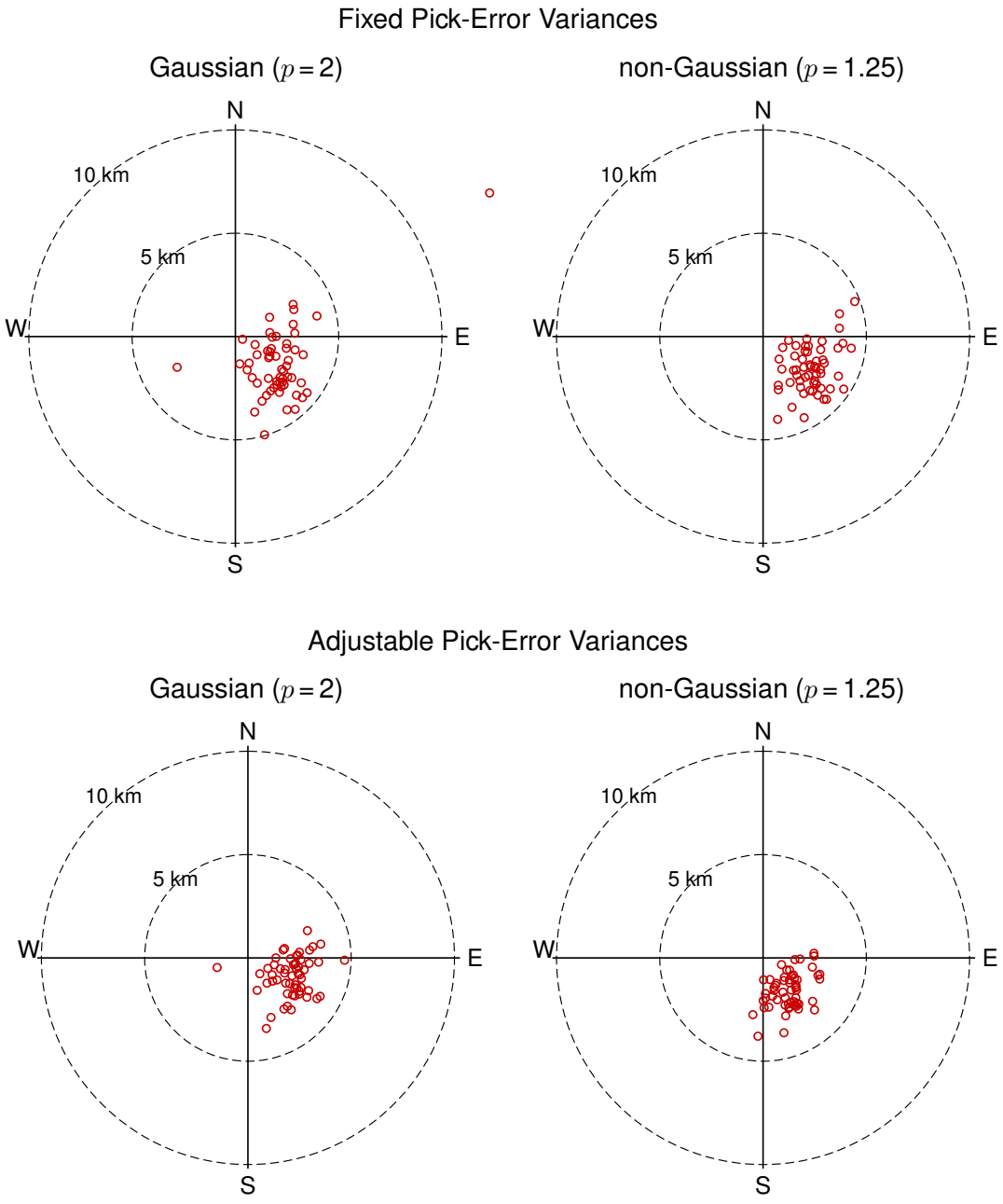

Figure 8: Mislocation vectors of GMEL solutions for the epicenters of 57 Pahute Mesa explosions, obtained with a variance-covariance matrix for travel-time corrections derived from geostatistical parameters for velocity heterogeneity. The results are shown in the same format and for the same four cases as Fig. 6.

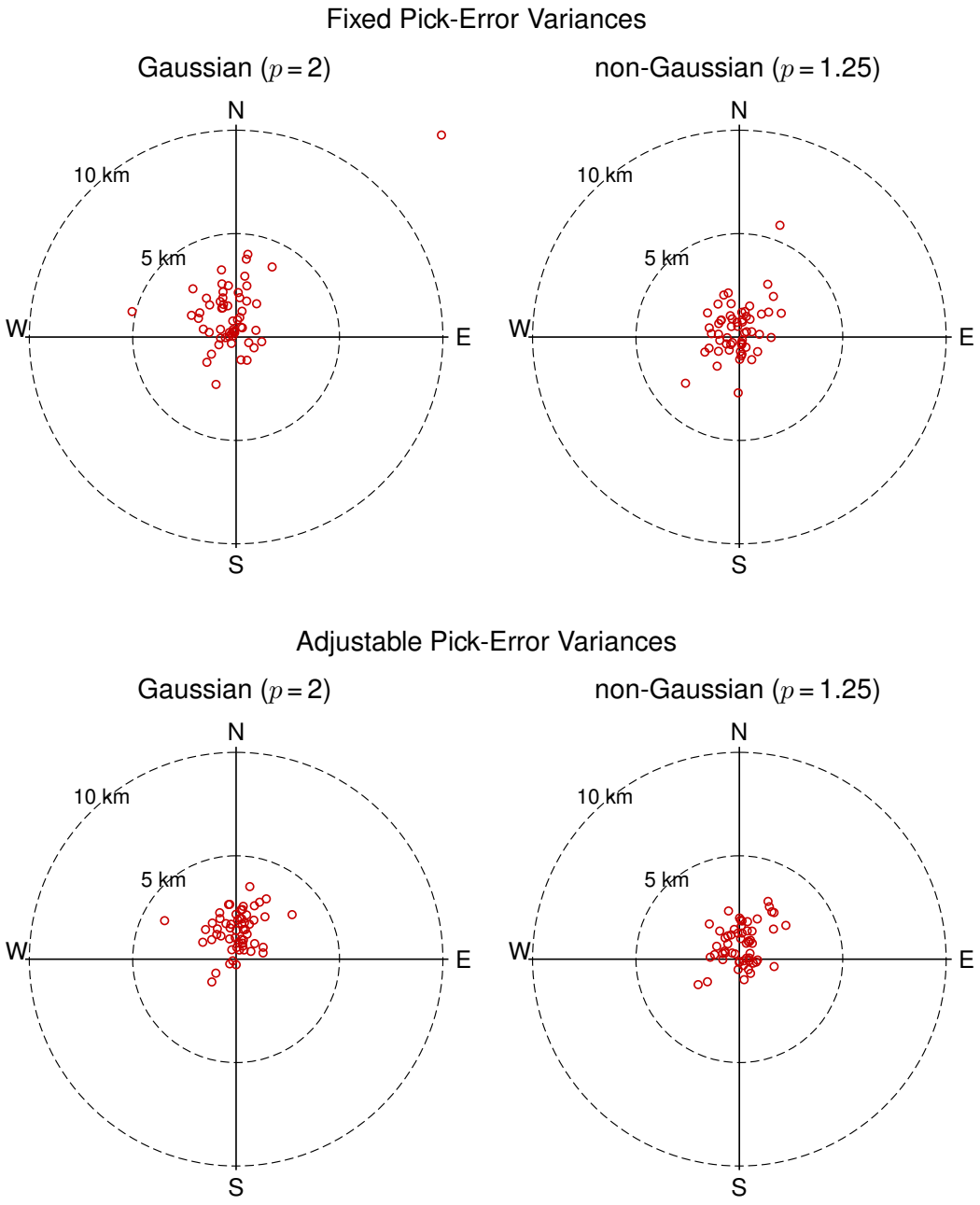

Figure 9: Same as Fig. 8 except the variance-covariance matrix for travel-time corrections was modified by setting the variances for local stations to zero, as was done for the diagonal variance matrix cases in Fig. 6.

5 CONCLUSIONS

The first year of the project was devoted largely to the development of our new multiple-event location methodology, including the mathematical formulation of the approach and implementation of key elements of the approach in the GMEL locator. The basic elements have been implemented and tested, resulting in numerical algorithms based on grid-search and nonlinear conjugate gradients to solve the multiple-event location problem under general stochastic assumptions about travel-time corrections and pick errors. Some important aspects of our approach await implementation, includ-ing uncertainty analysis within our more general framework and the extension to event-dependent travel-time corrections.

We tested our current version of GMEL with data from two event clusters in the IASPEI reference event list (REL). Application to the Rogun earthquake cluster in Tajikistan corroborated our theoretical conclusion that our general approach incorporates the HDC-RCA method as a special case. Application to a cluster of 57 explosions in the Pahute Mesa testing area of Nevada Test Site, for which GT0 location information is available, showed that our method can achieve epicentral locations with errors of 3 km and less when outlier suppression techniques we implemented are invoked, consisting of a non-Gaussian stochastic model for pick errors and automatic adjustment of pick-error variances. However, tests of our more general stochastic model of travel-time corrections, which employs a full variance-covariance matrix derived from a geostatistical characterization of unknown velocity anomalies in the Earth, did not reduce mislocation of the explosions at Pahute Mesa, indicating the need for further work on this element of our approach. We initiated efforts on the compilation of data sets for more clusters using the more complete International Seismological Centre's reviewed event bulletin, which will allow more exhaustive testing of our multiple-event location methodology in the second year of the project.

REFERENCES

Billings, S.D., M.S. Sambridge, and B.L.N. Kennett (1994), Errors in hypocenter location: picking, model and magnitude dependence, *Bull. Seism. Soc. Am.*, *84*, pp. 1978–1990.

Bonda´r, I., E.R. Engdahl, X. Yang, H.A.A. Ghalib, A. Hofstetter, *et al.*(2004), Collection of a reference event set for regional and teleseismic location calibration, *Bull. Seism. Soc. Am.*, *94*, pp. 1528–1545

Bonda´r, I., E. Bergman, E.R. Engdahl, B. Kohl, Y-L Kung, and K. McLaughlin (2008), A hybrid multiple event location technique to obtain ground truth event locations, *Geophys. J. Int.*, *175*, pp. 185-201.

Bonda´r, I. and K.L. McLaughlin (2009), A New Ground Truth Data Set For Seismic Studies, *Seis. Res. Ltrs*, *80*, pp. 465–472.

Engdahl, E.R. and E.A. Bergman (2001), Validation and generation of reference events by cluster analysis, *Proceedings*, 23rd Annual DoD/DOE Seismic Research Review, Jackson Hole, Wyoming.

Jordan, T.H. and K.A. Sverdrup (1981), Teleseismic location techniques and their application to earthquake clusters in the south-central Pacific, *Bull. Seism. Soc. Am.*, *71*, pp. 1105–1130.

Kelley, C.T. (1999), *Iterative Methods for Optimization*, Frontiers in Applied Mathematics, no. 18, Society for Industrial and Applied Mathematics, Philadelphia.

Kennett, B.L.N. (2006), Non-linear methods for event location in a global context, *Phys. Earth Planet. Int.*, *158*, pp. 46–54.

Kennett, B.L.N., E.R. Engdahl, and R. Buland (1995), Constraints on the velocity structure in the Earth from travel times, *Geophys. J. Int.*, *122*, pp. 108–124.

Myers, S.C., G. Johannesson, and W. Hanley (2007), A Bayesian hierarchical method for multiple-event seismic location, *Geophys. J. Int.*, *171*, pp. 1049-1063.

Myers, S.C., G. Johannesson, and W. Hanley (2009), Incorporation of probabilistic seismic phase labels into a Bayesian multiple-event seismic locator, *Geophys. J. Int.*, *177*, pp. 193-204.

Pavlis, G.L. and J.R. Booker (1983), Progressive multiple event location (PMEL), *Bull. Seism. Soc. Am.*, *73*, pp. 1753–1777.

Rodi, W. (2006), Grid-search event location with non-Gaussian error models, *Phys. Earth Planet. Int.*, *158*, pp. 55–66.

Rodi, W. (2008), Error analysis in the joint event location/seismic calibration inverse problem, AFRL-RV-HA-TR-2008-1016, Earth Resources Laboratory, Cambridge, MA.

Rodi, W.L. and S.C. Myers (2013), Computation of traveltime covariances based on stochastic models of velocity heterogeneity, *Geophys. J. Int.*, *194*(3), pp. 1582–1595.

DISTRIBUTION LIST

DTIC/OCP
8725 John J. Kingman Rd, Suite 0944
Ft Belvoir, VA 22060-6218 1 cy

AFRL/RVIL
Kirtland AFB, NM 87117-5776 2 cys

Official Record Copy
AFRL/RVBYE/Capt. Ashley Green 1 cy

This page is intentionally left blank.